Fault Ride-Through Strategy for Two-Stage GPV System Enabling Load Compensation Capabilities Using ANFIS Controller & EKF Algorithm

(THAMMATHU DHANASEKHAR REDDYBABU)[1](GODUGUCHINTA VENKAT PRADEEP)[2]

[1](M.TECH ELECTRICAL POWER SYSTEMS STUDENT), [2](ASST. PROFESSOR)

DEPARTMENT OF ELECTRICAL AND ELECTRONICS ENGINEERING,

SRI VENKATESWARA COLLEGE OF ENGINEERING AND TECHNOLOGY (AUTONOMOUS),

ANDHRA PRADESH, INDIA)

EMAIL ID: thammathu@gmail.com, venkatpradeep.g@gmail.com

Abstract:

This paper proposes an extended Kalman filter (EKF) based control strategy and ANFIS controller for fault ride-through operation in two-stage grid-connected photovoltaic (GPV) system. Unlike the conventional controllers for ride-through operation, the proposed strategy does not compromise with power quality improvement features in the system while enabling ride-through operation. The controller accounts for nonlinear loads in the system, grid harmonic-currents elimination and grid-currents balancing even during the harmonic/distorted grid voltages. The IEEE standard-1547.4 compels the distributed resource to ride-through during voltage disturbances caused by faults. For the ride-through operation, a limit is imposed on PV active power injection to prevent inverter over-currents and DC-link energy aggregation, which reduces the lifetime of DC-link capacitors. The reactive power is fed to the grid, as per the depth in voltage-sag. The de-rated PV array power is supplied in cases where the inverter cannot handle the utmost PV-power. The power quality improvement is ensured using EKF state estimator, which precisely estimates the fundamental load currents. In a distribution network with modern nonlinear loads, especially at far radial ends, the grid voltages are prone to huge diversions and the proposed controller provides a possible solution to maintain active/reactive power support and maintain power quality in the network. The effectiveness of the strategy is demonstrated through simulations. Under all disturbances, the harmonic content in grid currents is observed within limits, in accordance with the IEEE standard-519.

Keywords: Distributed generation, EKF, Total harmonic distortion (THD), Phase locked loop, PWM, ANFIS controller

.

I. INTRODUCTION

With the emphasis on clean power generation, the renewable energy based distributed generation systems have received great attention. Accounting to the recent developments in photovoltaic technology, the solar photovoltaic (PV) based renewable power generation has experienced a swift growth among the commercial and residential sectors [1]. However, increased dissemination of solar PV power generation into the traditional grid, has led to various power quality problems, especially in distribution networks where a significant portion of renewable energy sources are connected [2]. The advent of different power electronic loads further deteriorated the power quality in the network. Various solutions are proposed in the literature addressing the power quality issues without affecting the load profile [2]-[3]. There is a long tradition of using linear controllers for power quality improvement in grid-interfaced systems however they have their own limitations [4]. Moreover, these control schemes [4] necessitate phase locked loops (PLLs), which increases the system complexity in practical implementation and leads to mal-operation under distorted grid voltages. Recently, the power quality improvement in the distribution grid using nonlinear model predictive controllers (MPC), is contemplated by the authors in [5], however, its performance under nonlinear loads, is not investigated. To improve power factor and to minimize line current harmonics, modal reference adaptive control (MRAC) is introduced in [6]. However, it requires knowledge of the reference system a priori. These control strategies [3]-[6] focus on improving the power quality in the distribution network, with active/ reactive power injection to the grid. Their operation under gird-side faults, voltage unbalances and voltage harmonic distortions, is not analyzed.

On the other hand, there are control strategies for grid interfaced inverters for ride through operation during balanced/unbalanced voltage sag faults, without focusing on the power quality improvement in the dispersion network [7]-[12]. The scientists have accomplished the ride-through activity by infusing responsive force into the matrix. During the unbalance in dissemination network voltages, the guideline of grid current becomes challenging. The control algorithms are contemplated to overcome this issue, either by balancing the grid currents or by minimizing the active power fluctuations. For instance, the authors in [7] have developed a stationary frame PQ controller to minimize the ripple content in active power through a gain parameter. A synchronous frame current regulator is contemplated in [8]-[9] for power control during unbalanced grid voltages. The functionality of unbalanced voltage compensation using DG inverters is reported in [10]-[13], which are based on symmetric components. In these control strategies, the DG inverters are controlled either through positive sequence active powers or positive sequence reactive powers [11]-[12] or both positive sequence active and reactive powers [10]-[12] for compensating the unbalanced voltages. The studies have also been made for ride-through operation during unbalanced voltage sags with controllable active/reactive power oscillations. These strategies [7]-[12] depict different control approaches for ride-through operation in grid-interfaced distributed generation systems during grid voltage balanced/unbalanced sags. However, a) they fail to achieve the power quality improvement in distribution network through grid current harmonic compensation, b) they do not address the harmonic/distorted grid voltages caused at far radial ends in the distribution network, and c) they fail to address the dynamics of renewable energy resource (such as photovoltaic or wind) and the control of DC link voltage. The dynamics in PV arrays, DC-DC power conditioning stage and the DC-link capacitor, impact the operation of the overall system, especially during the fault ride through analysis and consequently, the task becomes challenging. The control strategies that consider dynamics of photovoltaic power plants are reported. The controller uses multiple proportional resonant (PR) controllers to achieve individual phase current compensation. The system performance with PR controllers is degraded under variation of the system frequency as it provides infinite gain at the selected harmonic frequencies. The non-ideal implementation of infinite gains could cause a series of instability issues for practical grid interfaced DG systems. Besides this, these strategies do not contribute for power quality improvement during nonlinear loads and harmonic voltages in the system. Moreover, the zero-sequence and negative-sequence powers are produced by unbalanced currents with unbalanced voltages, which badly affect different commercial loads and industrial loads connected at the higher end of the distribution system such as three-phase motor loads/ high power loads. The ride through operation of grid interfaced PV systems under low voltage sags, which ensures the different power-quality functionalities of harmonic current mitigation, power factor correction, balancing of grid currents, reliable operation during abnormal/harmonic grid voltages caused in distribution systems, is seldom reported in literature.

In this paper, the EKF scheme based double-stage grid-interfaced solar PV system is proposed, to accomplish manifold objectives. Firstly, the ride-through operation of grid-interfaced double-stage solar PV systems is evaluated under balanced/ unbalanced grid-side faults. During the grid faults, the PV inverter facilitates the quick detection and reacts accordingly to minimize the adverse effects on the inverter and grid-side equipment, to comply with IEEE Std. 1547.4. The system facilitates active and reactive power injection during the voltage-sag faults, so that the PV systems remain operational under such conditions without causing further instabilities due to loss of PV generation. Moreover, the proposed system is able to withstand the grid side harmonic/distorted voltages by supplying smooth and balanced sinusoidal grid currents. Contrary to many algorithms on ride through operation, the proposed control strategy is able to account for the nonlinear PCC loads in the distribution system, and compensates for the harmonic currents injected into the grid, even during the faults and harmonic voltage distortions. In this way, it satisfies the IEEE standard-519. The sinusoidal and balanced grid currents under all disturbances are ensured by incorporating a new way for extraction of unit-templates of grid voltages. This nullifies the negative sequence and zero sequence power injections into the grid during the grid voltage unbalances, thereby, the effect of sequence powers on industrial/commercial loads, is nullified. Besides this, a nonlinear Kalman filter is contemplated here. EKF is a mathematical method, which operates through prediction and correction mechanisms, and it estimates the fundamentals of the load current. It offers considerably better steady-state and dynamic performances, over the linear controllers, under system perturbations. It is a statistical technique and does not necessitate any dq-transformations, which are prone to errors if the synchronous frame identification is inaccurate, nor does it necessitates phase locked-loops. Its recursive structure allows real-time execution without storing observations or past estimates. The main contributions of the present work can be identified as follows.

- The fault ride through control strategy is presented for two-stage grid-interfaced solar PV system, that can handle harmonic/distorted grid voltages, caused at far radial ends in the distribution network, and still supply balanced and sinusoidal grid currents with THD with the limits depicted by IEEE Std. 519, despite severe voltage-sag faults.

- Contrary to several control strategies on ride-through operation, this control strategy accounts for nonlinear loads in the system, and compensates for unbalanced/harmonic loads during the voltage-sag faults and harmonic voltages.
- EKF control estimates the fundamental load currents, without the prior knowledge of amplitude, phase and behavior of the disturbances present in the load currents. The superior steady-state and dynamic performances of EKF based strategy over linear controllers are established.

The system is carefully evaluated through simulations and experiments. A prototype of two-stage grid interfaced PV system is developed in the laboratory and proposed control scheme is realized using DSP-dSPACE-1202 micro lab-box controller. Experimental results validate the steady-state and dynamic performances of the system under different test conditions.

II. SYSTEM CONFIGURATION

Fig. 1 shows the configuration of a double stage grid interfaced solar photovoltaic system with local loads connected at PCC (Point of Common Coupling). The system includes a PV array, three-phase voltage source inverter (VSI), the boost converter, interfacing inductors, DC link capacitor, ripple filter and the linear/nonlinear loads. The modeling methodology for PV array is reported in the literature. A two-stage system is considered here, where the DC-DC boost converter ensures the maximum power extraction from the PV array, using incremental-conductance (InC) based maximum power extraction technique, due the advantages it offers, in spite of a few demerits. In the InC algorithm, the direction of perturbation to reach maximum power point is decided by the difference between the incremental conductance and the conductance offered by the PV array.

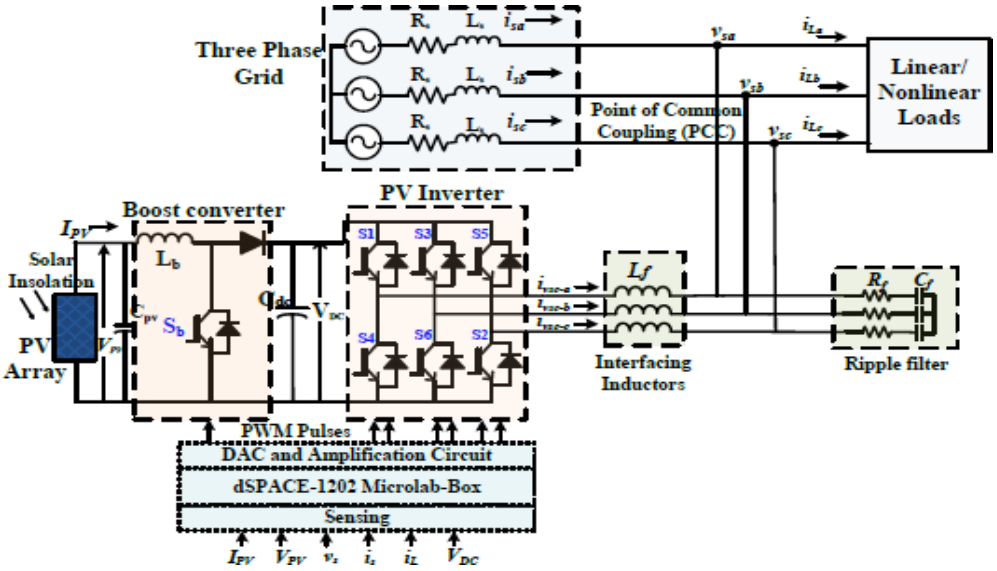

Fig.1. Configuration of two stage grid interfaced PV system

However, under severe grid side faults, the PV array is made to operate under non- MPPT mode, as the PV inverter cannot handle the maximum PV power. The ripples in the grid currents are eliminated using interfacing inductors and the VSI switching noises are absorbed by the ripple filter. The design and modeling procedure of the system is as presented in [2]. The details of system parameters are reported in Appendix.

III. CONTROL APPROACH

The systematic control for the grid interfaced power converter and the boost converter, are described here. The necessary inputs to the PV inverter, are grid currents (isa, isb, isc), load currents(iLa, iLb, iLc), PCC voltages (vsa, vsb, vsc) and the DC link voltage (VDC); whereas the boost converter controller primarily requires PV-array voltage (VPV) and current (IPV) as its sources of info. The reference network flows are assessed utilizing the control plot and the hysteresis controller is utilized to guarantee that the detected lattice flows follow the reference matrix flows. The overall control schematic for PV inverter is depicted in Fig. 2. The different objectives of the control are demonstrated by division of control into five modules namely, (i) load currents processing through EKF scheme, (ii) assigning the load current weights, (iii) evaluation of loss component and the PV feed forward

Component, (iv) Fault ride through control, and (v) generation of inverter gating pulses. These are explained as follows.

a. EKF Scheme for Load Currents Processing

The EKF scheme for estimation of fundamental components of load current, is described here. The KF is a mathematical procedure, which operates through prediction and correction mechanisms. It is a recursive structure that permits its continuous execution without putting away perceptions of past appraisals. It gives data about the nature of the estimation by giving, notwithstanding the best gauge, the fluctuation of the estimation error. The KF has the ability to correct itself and takes the advantage of corrections between unknown dynamics and updates itself. In essence, the KF algorithm predicts a new state from its previous estimation by adding a correction term proportional to predicted error. In this way, this error is statistically minimized.

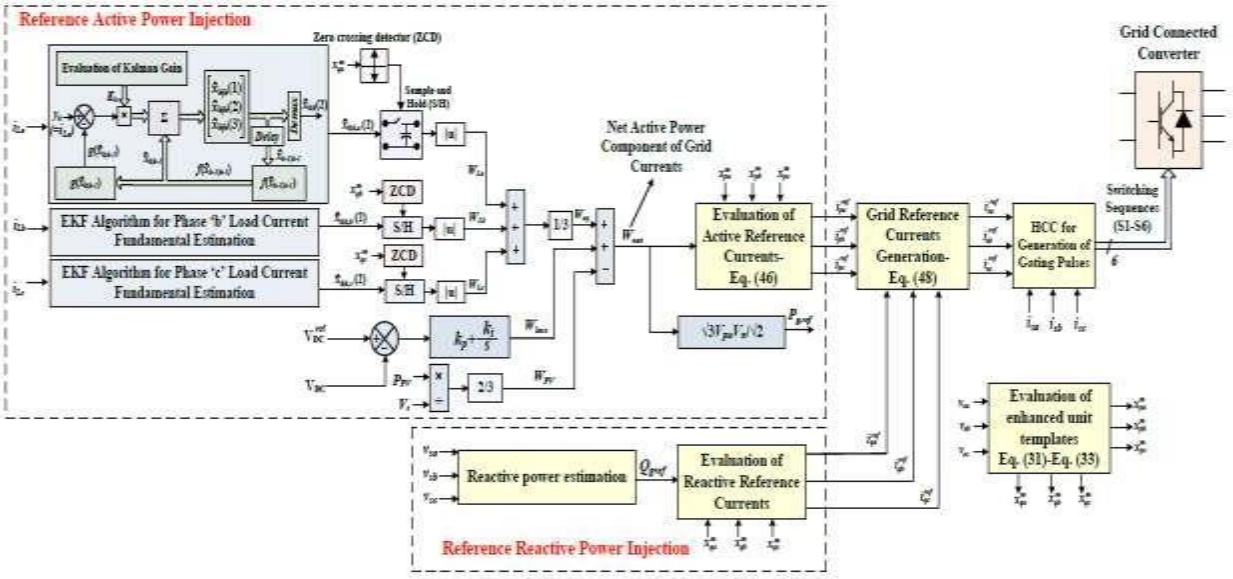

Fig.2. Control schematics for generation of PV invert gating pulses

Initially, the load current, is expressed as,

$$i_{La} = \sum_{n} I_{Lan} \cos\cos(\omega_n t + \emptyset_n) - - - (1)$$

Wherei_{pn}, $\emptyset_n$,ω_n are amplitude, phase and frequency of the nth harmonic component. The load current at kt sampling instant (yk), is expressed as,

$$y_k = I_{La1} \cos\cos K\omega_1 T_s + \emptyset_n + \varepsilon_k - - - (2)$$

Where, 'Ts' is the sampling time and εk is Gaussian noise with zero mean and variance $\sigma v2$. The expression (2) is stated in terms of estimated fundamental load current (y_k) as,

$$y_k = y_k + \varepsilon_k - - - -(3)$$

After considering three consecutive samples of load currents at sampling time Ts, the single sinusoid, „ " satisfies the following relationship, y_k

$$y_k - 2\cos\cos K\,\omega T_s y_{k-1} + y_{k-2} = 0 - -(4)$$

The estimated state-space vector at $(k-1)t$ instant is defined as,

$$x_{k-1/k-1} = [2\ cos\ cos\ \ k-1 \quad \omega T_s y_{-1} y_{-2}\ ]^T - (5)$$

The corresponding signal at kt instant can be identified as,

$$x_{k/k-1} = 10002\ cos\ cosK\omega T_s - 1010\ x_{k-1/k-1} - (6)$$

The $x_{k-1/k-1}$represents the estimated state variable at $(k-1)t$ instant with given values at $(k-1)t$ instant; and „$x_{k/k-1}$1" represents the estimated state variable at kth instant with given values at $(k-1)t$ instant. Thus, from (4)-(6), (3) can be expressed as,

$$y_k = 02\ cos\ cosK\omega T_s - 1\ x_{k/k-1} + \varepsilon_k - - - (7)$$

Nonlinear equations (6)-(7), are formulated as,

$$x_{k/k-1} = f(x_{k-1\ /k-1}\ )\ and\ y_k\ =\ g(x_{k\ /k-1}\ )\ + \varepsilon_k - - - (8)$$

Where,

$$f(x_{k-1\ /k-1}\ )\ =\ \ 10002\ \ cos\ cosK\omega T_s - 1010\ \ x_{k-1\ /k-1}\ \ - - - (9)$$

$$y_k\ =\ g(x_{k\ /k-1}\ )\ =\ \ 02\ \ cos\ cosK\omega T_s - 1\ x_{k/k-1}\ \ - - - (10)$$

The nonlinear recursive filter is applied to estimate the magnitude of the signal and its frequency even under presence of the noise, by linearizing the system (8)-(10) as,

$$x_{k/k-1} = f(x_{k-1\ /k-1}\ )\ - - - (11)$$

$$x_{k/k}\ = x_{k/k-1} + K_k(y_k - g(x_{k/k-1}))\ - (12)$$

Thus the estimated state vector $\hat{x}k|k$from (12), estimated for kt instant, is applied to the system. The Kalman gain (Kk) in (12) is evaluated as,

$$K_k\ =\ P_{k/k-1}\ \frac{\partial g^T}{\partial x}|(k/k-1)[\ P_{k/k-1}\ \frac{\partial g}{\partial x}|(k/k-1)\ P_{k-1}\ \frac{\partial g^T}{\partial x}|(k/k-1)\ + R_0]^{-1}\ (13)$$

The error covariance vector $P_{k/k-1}$ is evaluated and updated as follows.

$$P_{k/k-1} = \frac{\partial f}{\partial x}|(k/k-1)P_{k-\frac{1}{k}-1}\ \frac{\partial f^T}{\partial x}|(k/k-1) + Q_0 - - - (14)$$

$$P_{k/k}\ = P_{k/k-1}\ \ - K_k\ \frac{\partial g}{\partial x}|(k/k-1)\ P_{k/k-1}\ - (15)$$

$$\frac{\partial f}{\partial x}|(xk/x_{k/k-1})\ \ =\ \ 100x_{k/k-1}(2)x_{k/k-1}(1) - 1010\ \ (16)$$

$$\frac{\partial f}{\partial x}|(xk/x_{k/k-1})\ \ =\ [\ x_{k/k-1}(2)x_{k/k-1}(1) - 1]\ (17)$$

Here, Q_0 and R_0 are the covariance matrices associated with the process noise (wk) and the measurement noise (i.e.ε_k). The R_0 and Q_0 for EftF, are typically initialized as 10−4 and 10−4I3×3, respectively [29].

In (13), however, $R_k = R_0\ e^{\frac{y_k - g\ x_{\frac{k}{k}-1}}{2}}$ is considered instead of Ro, by assigning the exponential term of error between sensed load current and estimated fundamental load component, to the error covariance term. If the error between sensed and estimated components is high, then, the exponential factor increases faster, which increases the

error covariance term and mitigation of error is achieved. Thus, robust performance of the EKF is achieved by incorporating exponential terms, under high disturbances in the load current.

The state prediction is used to compute the value at time point k based on the estimated value at time point k-1. If current dynamics is largely varied at time point k-1, the estimator is not capable of following the situation and provides appropriate weighting. As a result, it is not capable to predict a value that is close to the real value at time point k. Nevertheless, the algorithm still outputs the appropriate value, because the innovation vector $(y_k - g(x_{k/k-1}))$ swiftly changes under such conditions, amplifying the Kalman gain. The estimated three phases fundamental load currents $x_{k/k,a}$ (2), $x_{k/k,b}$ (2), $x_{k/k,c}$ (2) are thus obtained and processed further to generate the switching pulses of VSI. The block diagram representing the process is shown in Fig. 3.

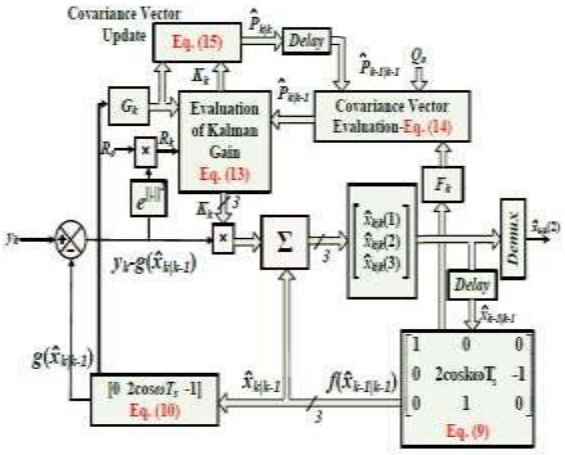

Fig. 3 Implementation of EKF algorithm

As depicted earlier, the estimated state vector $\hat{x}\ k|k$from (12), is estimated for kth instant, is the output of the EKF control. Its deviation from the actual state vector at kt instant (xk) is the error, i.e.

$$e_{k/k} = x_k - x_{\ k/k} - - - (18)$$

The corresponding error at $(k-1)t$ instant can be identified as,

$$e_{k/k-1} = x_k - x_{\ k/k-1} - - - (19)$$

From (11)-(12), the formulations (18)-(19) are as,

$$e_{k/k} = F_{k-1}e_{k/k-1} + n_k + l_k - - - -(20)$$

$$e_{k/k-1} = F_{k-1}e_{k-1/k-1} + w_{k-1} + r_{k-1} - -(21)$$

Where, $rk-1$is the remainder term at $(k-1)^t$ instant $(e_k - F_{k-1}\ I_{3X3} - K_k G_{k-1}\ e_{k-1})$ and

$$F_{k-1} = [I_{3X3} - I_{3X3} - K_k G_{k-1}\ e_{k-1})] - -(22)$$

$$n_k = I_{3X3} - K_k G_{k-1}\ w_{k-1} - K_k \varepsilon_k - - - (23)$$

$$l_k = I_{3X3} - K_k G_{k-1}\ r_{k-1} - - - -(24)$$

$$F_{k-1} = \frac{\partial f}{\partial x}|(x_{k/k-1}); G_{k-1} = \frac{\partial g}{\partial x}|\ x_{k/k-1} \text{ --- (25)}$$

With the decent assumptions that the norm $|F_k|$ is bounded and $P_{k/k}$ and $P_{k/k-1}$ are bounded with$P_1 I_{3X3}$, $P_2 I_{3X3}$ and $q_1 I_{3X3}$,$q_2 I_{3X3}$ as respective lower and upper bounds. The following lemmas can be identified to prove the exponential convergence of the algorithm [30].

Lemma-1: With Fk as non-singular ∀k>0, and $|F_k|$ $P_{k/k}$ and $P_{k/k} - 1$ are bounded, then there exist a real number 0 <λ<1 such that,

$$F_k^T P^{-1}{}_{k/k-1} F_k \leq 1 - \lambda\, P^{-1}{}_{k/k-1} \quad ---(26)$$

Lemma-2: When the ratio of largest and smallest singular value in „Gk" matrix has an upper bound „g", then an upper bound for the norm of the Kalman gain matrix is given as,

$$|F_k| \leq g \frac{q_2}{q_1} --(27)$$

Thus, when the error at $(k-1)t$ instant i.e. $|e_{k-1/k-1}|$ is bounded, with the bounds (26) and (27), it can be proved that the solution of the error model (20) is exponentially stable with finite bounded limits [30].

b. Assigning Load Current Weights

The active power component of load currents is then evaluated using a sample and hold (S/H) control logic. The fundamental component estimated from (8)-(17), is passed through S/H logics. Since the fundamental component is in phase with the grid voltages, the triggering pulses for S/H logics are produced using quadrature unit templates, with a zero crossing detector (ZCD). This is described in Fig. 2. For this purpose, the in-phase (xpa, xpb, xpc) and quadrature (xqa, xqb, xqc) unit templates are computed. To achieve satisfactory performance under grid voltage imbalances and harmonic distortions, a new method of extraction of unit templates is presented here. The mathematical formulation for derivation of enhanced unit templates follows the following sequence.

1) Initially the positive sequence phase voltages are evaluated. The instantaneous positive sequence voltage components in αβ reference frame are evaluated as,

$$V_{\alpha\beta}^{+} = T_{\alpha\beta}\, T_p\, T_{\alpha\beta}\, V_{\alpha\beta} = \frac{1}{2} 1 - e^{-j\pi/2} \quad e^{-j\pi/2}\, 1\, V_{\alpha\beta} - (28)$$

$$T_{\alpha\beta} = \sqrt{2/3}\, 1 - 0.5 - 0.500.866 - 0.866 --(29)$$

$$T_p = \frac{1}{3} 1aa^2a^211aa^21\,;\, a = e^{j2\pi/3} --(30)$$

Thus, from (28) the positive sequence voltages „$V_{\alpha\beta}^{+}$" and corresponding quantities in abc −domain, are evaluated using inverse Clarke's transformation. The implementation of (28) is depicted in Fig. 4. Initially, αβ-components of phase voltages ($v\alpha, v\beta$) are generated through Clarke's transformation. These are processed through generalized integrators of second order, to obtain corresponding in-phase ($v\alpha i, v\beta i$) and quadrature ($v\alpha q, v\beta q$) components.
The description of second order- second order generalized integrators (SO-SOGI) is reported in [31]. The in-phase and quadrature components are further possessed, as shown in Fig. 4, to evaluate the balanced positive sequence voltage components($vsa+, vsb+, vsc+$).

2) The amplitude of terminal voltage is then evaluated as,

$$V_t = \sqrt{\frac{2}{3}\left(v_{sa}^{+2} + v_{sb}^{+2} + v_{sc}^{+2}\right)} ----(31)$$

3) The enhanced in-phase ($(xpa\,m, xpb\,m, xpc\,m)$) and quadrature ($(xqa\,m, xqb\,m, xqc\,m)$) unit templates are then computed as,

$$x_p^m = [x_{pa}\, x_{pb}\, x_{pc}]^{m\,m\,m\,T} = \frac{1}{V_t}[v_{sa}\, v_{sb}\, v_{sc}]^{+\,+\,+\,T} \quad -(32)$$

$$x_q^m = x_{qa}^m\, x_{qb}^m\, x_{qc}^m = \frac{1}{2\sqrt{3}} 0 - 2231 - 131 - 1\, x_{pa}^m\, x_{pb}^m\, x_{pc}^m - (33)$$

Finally, the load current weights (WLa, WLb, WLc) are obtained from S/H logics output. The average of load current weight, is the equivalent active power component of load current($WLex$).

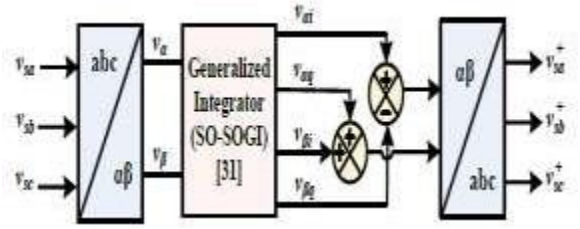

Fig. 4 Evaluation of balanced positive sequence grid voltages

c. DC Link Voltage Regulation and PV Feed-Forward Compensation

The PV inverter requires dynamic capacity to manage DC connect voltage (VDC) to its reference ($VDC\ ref$). The VSC expends some force from a typical coupling point during variety of the DC connect voltage, which is known as a misfortune part of dynamic power ($Wloss$). It is utilized to control DC interface voltage as indicated by reference DC connect voltage, and is assessed as,

$$w_{loss} = K_p \left(V_{DC}^{ref} - V_{DC}\right) + K_i \int \left(V_{DC}^{ref} - V_{DC}\right) dt \quad (34)$$

Where, 'KP' and 'ki' are the corresponding and basic editions of the controller, individually. The reference voltage for DC connect capacitor is kept 1.2 occasions the pinnacle of the line voltage. Additionally, PV feed-forward term is incorporated here, to quicken the dynamic response under continuous solar insolation fluctuations that occur in practical PV systems. A practical grid-interfaced PV system is subject to continuous variation of solar isolation. A fast dynamic response is desired under such continuous disturbances to the system. This is facilitated by the feed-forward term (WPV) by minimizing the transients in the grid currents. The PV feed-forward is an additional term accommodated in the control strategy, which adjusts the reference grid currents without any feedback from the controller, to improve the dynamic performance of grid currents during the changes in solar insolation. Since the dynamics are directly associated with the change in PV array power (P_{PV}), „W_{PV} " can be identified as,

$$W_{PV} = \frac{2P_{PV}}{3V_t} - - (35)$$

d. Fault Ride-Through Control

The proposed fault ride-through control of PV inverter is demonstrated in this section. The three phase voltages are communicated in $\alpha\beta$ reference outline utilizing Clarke's change grid portrayed in (36) (where $u\alpha\beta$ is a vector in $\alpha\beta$ reference casing and $uabc$ is a vector in abc reference outline).

$$u_{\alpha\beta} = T^{abc}_{\alpha\beta} u_{abc}, T^{abc}_{\alpha\beta} = 2/3\ 1 - 1/2 - 1/20\ 3/2 - 3/2 - \quad (36)$$

The αβ-voltage components, „$v\alpha$" and „$v\beta$" are used to compute their respective positive and negative sequence voltages as follows,

$$\begin{matrix} V^+_\alpha & V^+_\beta & V^-_\alpha & V^-_\beta \end{matrix} = \frac{1}{2} \begin{matrix} 1 - e^{-j\pi/2} & e^{-j\pi/2} \\ 1 & -e^{-j\pi/2} \end{matrix} \begin{matrix} e^{-j\pi/2} \\ 1 \end{matrix} \begin{matrix} 1 - 1/2 - 1/2 \\ 0\ 3/2 - 3/2 \end{matrix} \begin{matrix} \\ V \end{matrix} \quad \begin{matrix} \\ V_{sa}\ V_{sb}\ V_{sc} \end{matrix} \quad (37)$$

The positive sequence voltage$(V+)$, negative sequence voltage $(V-)$ and the per-unit voltage (Vpu) are then computed as follows,

$$V^+ = \sqrt{V^{+2}_\alpha + V^{+2}_\beta}; V^- = \sqrt{V^{-2}_\alpha + V^{-2}_\beta}$$

$$V^+ = \left(3/2V_n\right) \sqrt{V^{+2}_\alpha + V^{+2}_\beta}$$

$$; V_{pu} = Mean(V_{pu}) \quad (38)$$

Where „Vn" is the nominal converter voltage. The over currents caused due to the near PCC faults, trip the interfacing power converter thereby leading to the loss in entire solar PV generation. To avoid such failures, inverter

nominal power must be updated under low voltages. Therefore, a modified nominal power (MNP), is adopted here, which is a function of voltage sag depth and nominal converter power (Sn) as,

$$MNP = \frac{1}{Vn} V^{+} - V^{-} Sn - - - - - (39)$$

Under low voltage faults in the system, the modified power is updated to take a value lower than the nominal power of the converter. The decrease in voltage magnitudes of either single phase, double phase or three phase voltages, results in a decrease in the value of MNP. This is demonstrated in more detail in the simulation results. As per the depth of voltage drop, the estimated reactive power entering the grid (QgE) to be supplied by the converter is decided as follows,

$$Q_{gE} = \{0 \; if \; \underline{V}_{pu} > 0.9 \; 1.35 - 1.5 V_{pu} \; Sn \; if \; 0.2 < V_{\underline{pu}} < 0.9 1.05 Sn \; if \; V_{\underline{pu}} < 0.2 \; (40)$$

Thus the maximum active power injection, for a given value of MNP and reactive power can be identified as,

$$Pmax = \{\overline{MNP^2 - Q^2} \; if \; MNP > Q_{gE} \; 0 \; if \; MNP < Q_{gE} \; (41)$$

Under normal conditions, the reference grid reactive power ($Qgrep$) is „Q_{gE} ", governed by (40), However, under very deep voltage sags, the VSI is incapable of injecting the reactive power higher than the MNP, and therefore, the converter is made to supply reactive power equal to MNP. Thus,

$$Q_{gref} = \{Q_{gE} \; if \; MNP \geq Q_{gE} \; MNP \; if \; MNP < Q_{gE} - -(42)$$

Therefore, as long as, the $Pmax$ i.e. (41) is higher than the greatest force point reference ($Pref$) given by the MPPT controller, the most extreme force can be infused from the PV exhibit to the framework. As referenced before, an InC calculation is utilized for most extreme force point following purposes, where the course of bother to arrive at greatest force point is chosen by the contrast between the gradual conductance ($dIPV/dVPV$) and the conductance (IPV/VPV) offered by the PV array. When the difference is positive, it identifies the operating point as left of the PV curve and tries to shift the operating point to the right. The visa-versa is true in the case when the difference is negative. Along these lines, the reference PV cluster voltage is assessed dependent on the InC standard the comparing obligation proportion of the lift converter is assessed. Be that as it may, on the off chance that $Pmax$ is lower than the$Pref$, at that point the PV array is made to operate in de-rated mode, at a new operating point corresponding to a new value of active power i.e. $Pmax$. The de-rated operation of PV array is depicted in Fig. 5, where the boost converter is controlled to operate in non-MPPT mode. As shown in Fig. 5,

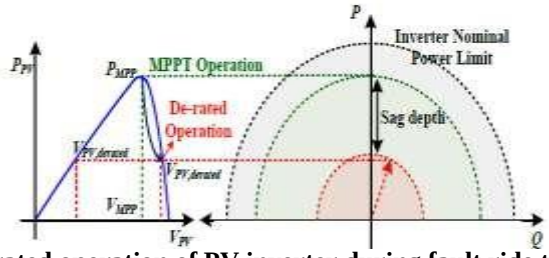

Fig.5. De-rated operation of PV inverter during fault ride through operation

The right hand side operating point is considered here, as the operating point can move faster on the high ramp side of the P-V curve. The reference obligation proportion of the lift converter is along these lines gotten under typical and de-evaluated conditions as follows,

$$D_{nor\ mal} = 1 - \frac{V_{PV}^{ref}}{V_{DC}} \; - - - \; 43$$

$$\square \quad _{derated} = \frac{Pmax}{Pref} \quad 1 - \frac{_{PV}V^{ref}}{V_{DC}} - -(44)$$

Where $'VPV\ ref\ '$ is the reference PV-voltage voltage given by the MPPT controller. The control of the lift converter is shown in Fig. 6. Under typical conditions, the lift converter is made to operate in MPPT mode.

However, the de-rated operational mode is activated as soon as low voltage is detected (below 0.9pu) and $Pmax < Pref$. The duty ratio thus obtained, is compared with the high frequency carrier signal for the generation of switching pulses to the boost converter. The proportional-integral controller in de-rated operation, tunes new duty cycle to precisely follow „$Pmax$".

e. Generation of Inverter Gating Pulses

The gating pulses for PV inverters are generated using active and reactive reference grid currents. For this purpose, the net active power component ($Wnet$) is evaluated. The net active power segment of the current segment is the abundance of reference lattice flows. This is evaluated by summation of comparable burden dynamic force part weight with the abundances of the reference inverter currents (45), in accordance with the Kirchhoff current law at PCC. Thus „$Wnet$" can be identified as,

$$W_{net} = W_{eq} + W_{loss} - W_{PV} ----(45)$$

SinceW_{net} " is the net active current weight; the reference active power delivered by the grid ($Pgref$) is obtained by multiplyingW_{net} " with $3\overline{V_{pu}}V_n/2$. Where, „Vn" is the nominal grid voltage. This is because the active current weight ($Wnet$) is the peak amplitude of the active current, i.e.

$$Pg = 3\overline{V}_{rms} I_{active,rms} = (3\overline{V_{pu}} V_n / 2)\overline{W}_{net}$$

. The active reference currents are then evaluated as,

$$i_p^{ref} = [\, i_{pa}^{ref} \; i_{pb}^{ref} \; i_{pc}^{ref} \,]^T = W_{net} X_p^m ----(46)$$

To evaluate the reactive reference currents, the reactive current weight (Wq) is obtained by scaling the reference reactive power determined from (42) with the magnitude of terminal voltage. The reactive reference currents are then obtained as

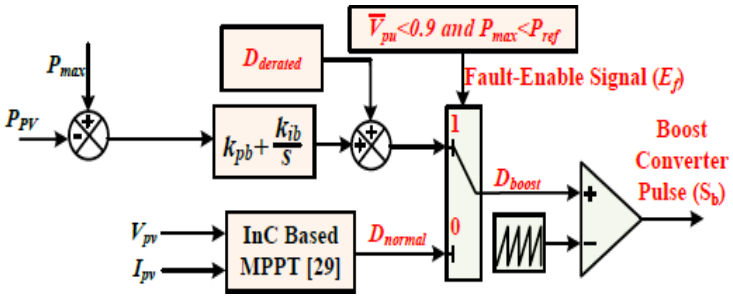

Fig. 6 Control schematic for generation of boost converter gating pulses

$$i_q^{ref} = [\, i_{qa}^{ref} \; i_{qb}^{ref} \; i_{qc}^{ref} \,]^T = W_q X_q^m ----(47)$$

Finally, the reference grid currents are generated as,

$$i_s^{ref} = [\, i_{sa}^{ref} \; i_{sb}^{ref} \; i_{sc}^{ref} \,]^T = i_p^{ref} + i_q^{ref} ----(48)$$

The error between reference grid currents (48) and the sensed grid currents is infiltrated through the hysteresis current controller (HCC) to produce the inverter gating pulses.

COMPARATIVE STUDY WITH EXISTING ALGORITHMS

Different control approaches for both grid-interfaced distributed generation systems and specifically solar-PV systems with their advantages/ disadvantages are analyzed in the introduction section. With fault ride through capability, the control strategies for PV systems involve multifunctional features. On the other hand, the controller actions of the proposed controller are discussed in section-III. A comparison is made herein with the multifunctional strategies, from the functionalities point of view. The topology proposed is for a neutral-point clamped inverter. The proposed control strategy is proposed for a distribution level system. From functionalities point of view, both approaches have achieved inverter reference current control with reactive power injection during both

balanced/unbalanced voltage sages, while ensuring the inverter peak current limit capability. However, the proposed strategy is advantageous over these controllers as it offers significant additional functionalities, which include harmonic currents mitigation, power factor correction and balancing of grid currents. Moreover, unlike the conventional algorithms, the system operation with the proposed strategy is not affected by abnormal/harmonic grid voltages caused at far radial ends in the distribution system.

IV. ANFIS controller:

A fuzzy based controller and a back spread calculation. For a conventional fuzzy method, the parameters in the enrollment limits are commonly directed by comprehension or the experimentation technique. In any case, the adaptive neuro-fuzzy inference controller can vanquish this shortcoming through the path toward creation sense of how to modify the support abilities to the data/output data remembering the ultimate objective to express to these sorts of assortments in the data regards, rather than discretionarily picking parameters related with a given enrollment work. This learning strategy works likewise to that of neural frameworks.

The Adaptive Neural Fuzzy Inference System (ANFIS) is a fuzzySugeno show placed in the structure to energize learning and alteration strategy. Such a framework makes fuzzy basis all the more deliberate and less relying upon controlling data. The objective of ANFIS is to change the parameters of a fuzzy framework by applying a learning strategy using input–output planning data. Basic structure of ANFIS that has two data sources x and y and one output f. In Mat lab the essential differentiation between fuzzy controller and adaptive neuro fuzzy controller is simply we have in Mat lab two composes fuzzy controllers one is Mamdani and second one is Sugeno.

Mamdani a normal fuzzy controller in this we give data and output by using a couple of suppositions yet in Sugeno create we give inputs just they normally get ready outputs this is the essential complexity between two fuzzy controllers in MATLAB. So Mamdani created a fuzzy controller used as a standard fuzzy controller and a Sugeno compose fuzzy controller used as an adaptive neuro fuzzy controller in the MATLAB.

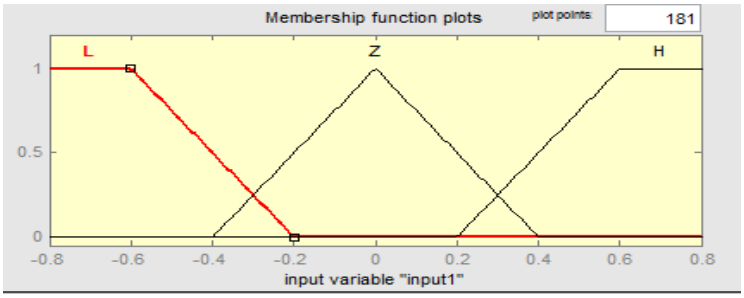

Fig.7. Membership function of error

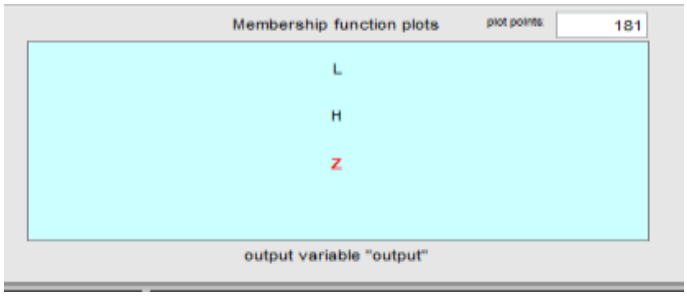

Fig.8. Output membership functions

Input	Output
L	L
G	G
H	H

Table:1 ANFIS rules

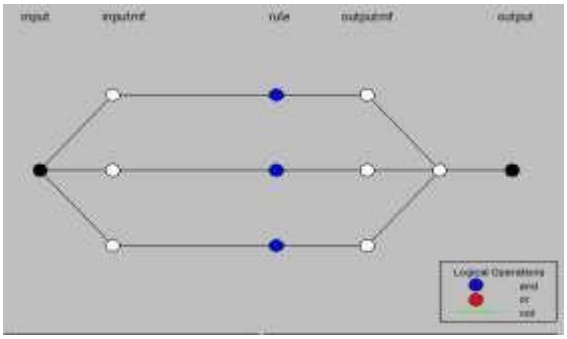

Fig: 9. ANFIS model based structure

V. Simulation results:

a) Simulation results using pi controller:

To verify the pi based control scheme, a simulation test-bed is built in the MATLAB®-Simulink based environment with Sims cape toolbox. A 415V, 50Hz system is considered here, with DC link voltage of 1.2 times the peak of line voltage. This section describes the system performance under grid-side faults, highlighting the salient signals. The performance of grid interfaced PV systems under low voltage faults is depicted in Fig. 10. The simulation parameters are reported in Appendix. Single line to ground (L-G) and double-line to ground (L-L-G) faults, are simulated at 1s and 1.1s, respectively. Upon the occurrence of the fault, the per-unit voltage falls to 0.6pu. A severe L-L-G fault is then simulated at 1.2s where the grid voltages fall as low as 0.1pu. The salient signals of grid voltages (vg),$V+-V-$, Vpu,MNP,$Pmax$,Qg, , $Dboost$, PPV, VPV, grid currents (ig) and VSC currents ($iVSC$) are depicted in Fig. 10. As soon as fault signal is detected by the algorithm, $V+-V-$, MNP and $Pmax$ are updated as per (38),(39) and (41), respectively. These are shown in Fig. 10(a). The reactive power injected to the grid, follows the reference reactive power (42), and thereby provides the reactive power support under low voltage faults. As soon as the MNP falls below the rated power of the power–converter (35 kVA), the de-rated PV array operation mode is enabled. Consequently, the duty ratio is updated as per (43)-(44) (Fig. 6). The PI control parameters ($kpb\ and\ kib$) are reported in Appendix. Accordingly, the dynamics in duty ratio of the boost converter ($Dboost$), PV voltage (Vpv) and PV array power (Ppv) are observed as shown in Fig. 10(b). Before the occurrence of the fault, the PV array operates at its MPP of 440V and 30kW, however, the PV power is limited to $Pmax$(25kW and 19kW), after the occurrence of faults at 1s and 1.1s, and Vpv is shifted to new operating points at 500V and 522V, respectively. It may be noted from Figs. 10(a)-(b) that, under severe grid faults (at 1.2s), the reactive power entering the grid (Qg) is limited to MNP (3.5 kVA). In this case, no active power supplied by the PV inverter, with zero duty-ratio of the boost converter; thus, the PV inverter simply acts as a static compensator. Despite the unbalanced voltage faults, the grid currents always remained balanced and sinusoidal with THD less than 5%, as the compensating currents are provided by the PV inverter under all conditions.

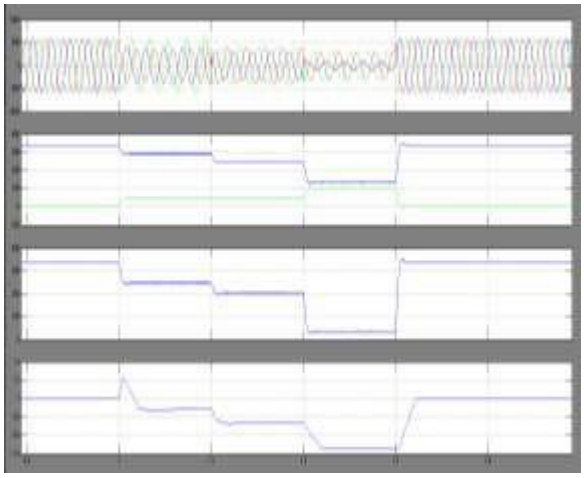

a. Vsabc, V^+ &V^-, V^+-V^-, Vpu

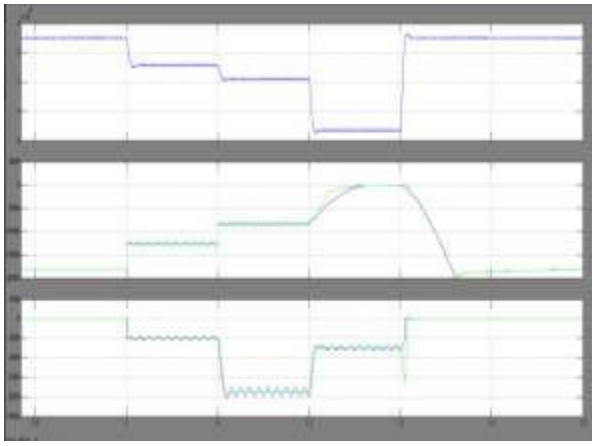

MNp, Pg, Qg

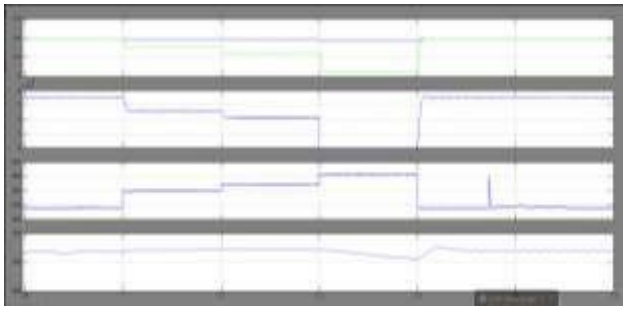

Boost max, Vpv, Vdc

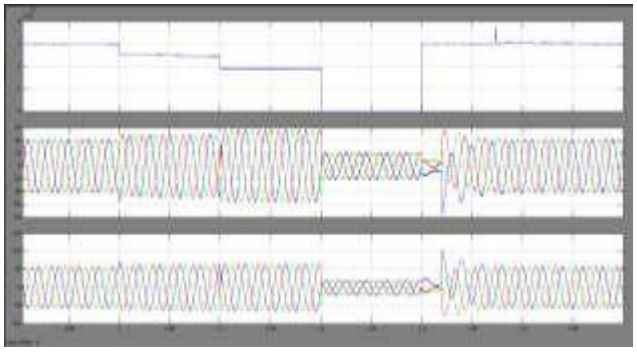

Ppv, Isabc, Ivsc

Fig. 10 System response under L-G and L-L-G faults depicting fault ride-through operation of PV inverter

b) Simulation results using ANFIS controller:

To verify the proposed control scheme, a simulation test-bed is built in MATLAB®-Simulink based environment with Sims cape toolbox. A 415V, 50Hz system is considered here, with DC link voltage of 1.2 times the peak of line voltage. This section describes the system performance under grid-side faults, highlighting the salient signals.

The performance of grid interfaced PV systems under low voltage faults is depicted in Fig. 11. The simulation parameters are reported in Appendix. Single line to ground (L-G) and double-line to ground (L-L-G) faults, are simulated at 1s and 1.1s, respectively. Upon the occurrence of the fault, the per-unit voltage falls to 0.6pu. A severe L-L-G fault is then simulated at 1.2s where the grid voltages fall as low as 0.1pu. The salient signals of grid voltages (vg), $V+-V-$, Vpu, MNP, $Pmax$, Qg, $Dnormal$, $Dboost$, PPV, VPV, grid currents (ig) and VSC currents ($iVSC$) are depicted in Fig. 11. As soon as fault signal is detected by the algorithm, $V+-V-$, MNP and $Pmax$ are updated as per (38),(39) and (41), respectively. These are shown in Fig. 11(a). The reactive power injected to the grid, follows the reference reactive power (42), and thereby provides the reactive power support under low voltage faults. As soon as the MNP falls below the rated power of the power converter (35 kVA), the de-rated PV array operation mode is enabled. Consequently, the duty ratio is updated as per (43)-(44) (Fig. 6). The PI control parameters ($kpb\,and\,kib$) are reported in Appendix. Accordingly, the dynamics in duty ratio of the boost converter ($Dboost$), PV voltage (Vpv) and PV array power (Ppv) are observed as shown in Fig. 11(b). Before the occurrence of the fault, the PV array Operates at its MPP of 440V and 30kW, however, the PV power is limited to $Pmax$(25kW and 19kW), after the occurrence of faults at 1s and 1.1s, and Vpv is shifted to new operating points at 500V and 522V, respectively. It may be noted from Figs. 11(a)-(b) that, under severe grid faults (at 1.2s), the reactive power entering the grid (Qg) is limited to MNP (3.5 kVA). In this case, no active power supplied by the PV inverter, with zero duty-ratio of the boost converter; thus, the PV inverter simply acts as a static compensator. Despite the unbalanced voltage faults, the grid currents always remained balanced and sinusoidal with THD less than 5%, as the compensating currents are provided by the PV inverter under all conditions.

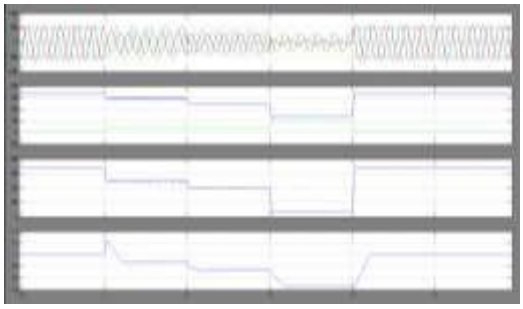

a. Vsabc, V^+ &V^-, V^+-V^-,Vpu

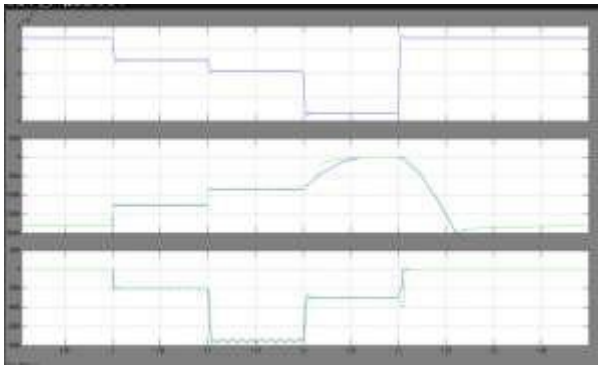

b. MNp,Pg,Qg

c. Boost max, Vpc, Vdc

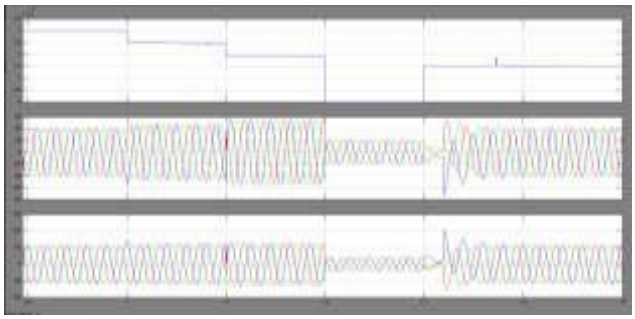

d. Ppv,Isabc,Ivsc

Fig. 11 System response under L-G and L-L-G faults depicting fault ride-through operation of PV inverter

VI. Conclusion:

The EKF state-estimator based control strategy and ANFIS controller is proposed for fault ride through operation in two-stage grid interfaced PV system, which enables the load compensation features in three phase distribution system. The converter over-currents caused due to low voltage sags in the GPV system, are avoided, by providing an auxiliary reactive power support as recommended by IEEE Standard-1547.4. Here, the ride-through operation is achieved without compromising the load compensation features such as grid harmonic currents elimination, grid currents balancing and power factor correction. For ride-through purpose, a maximum safe limit of PV power injection is derived as a function of grid-voltage sag and the PV inverter rating. The de-rated operation of PV array is enabled, in cases when the maximum PV power becomes higher than the maximum safe limit of active power injection. To achieve this, the mechanism for a boost converter duty-ratio control is presented. The reactive power is then injected to the grid under voltage sag faults, as per the depth in voltage-sag. The simulation results under LG and LLG faults, demonstrate the effectiveness of the proposed control scheme. Despite the unbalanced faults, the grid currents remain balanced and sinusoidal, thereby, the negative sequence and zero sequence power injection to the grid are avoided. Test results validate proposed control strategy. The features of harmonic currents mitigation, reactive power compensation, grid currents balancing and power factor correction, are illustrated under various test conditions. The results under distorted grid voltages and L-G unbalanced fault, are also presented. Under both normal and abnormal grid conditions, the grid currents with proposed control strategy are balanced and are maintained within the THD limit recommended by the IEEE standard-519. The practical grid interfaced PV systems are subject to continuous grid side perturbations and proposed control strategy serves as a possible solution, owing to its multi-functional features and self-adaptation capability to the variations in grid-side parameters.

VII. References:

1) E.Hache, A. Palle, “Renewable energy source integration into power networks, research trends and policy implications: A bibliometric and research actors survey analysis”, Energy Policy, vol. 124, pp. 23-35, 2019.
2) B. Singh, A. Chandra, and K. Al-Haddad, Power Quality: Problems and Mitigation Techniques. Hoboken, NJ, USA: Wiley, Jan. 2015.
3) V. L. Srinivas, S. Kumar, S. Bhim and S. Mishra, "A Multifunctional GPV System Using Adaptive Observer Based Harmonic Cancellation Technique," IEEE Trans.Ind. Electron. vol. 65, no. 2, pp. 1347-1357, 2018..
4) S. Bhim and J. Solanki, “A comparison of control algorithms for DSTATCOM,” IEEE Trans. Ind. Electr., vol. 56, no. 7, pp. 2738-2745, July 2009.
5) Q. Chen, X. Luo, L. Zhang and S. Quan, “Model predictive control for three-phase four-leg grid-tied inverters,” IEEE Access, vol. 5, pp. 2834-2841, 2017.
6) K. K. Shyu, M. J. Yang, Y. M. Chen and Y. F. Lin, "Model Reference Adaptive Control Design for a Shunt Active Power Filter System," in Proc. IECON 2006 - 32nd Annual Conference on IEEE Industrial Electronics, Paris, 2006, pp. 73-78.
7) W. Fei, J. L. Duarte, and M. A. M. Hendrix, “Pliant active and reactive power control for grid-interactive converters under unbalanced voltage dips,” IEEE Trans. Pow. Electr., vol. 26, no. 5, pp. 1511–1521, 2011.
8) H. S. Song and K. Nam, “Dual current control scheme for PWM converter under unbalanced input voltage conditions,” IEEE Trans. Ind. Electron., vol. 46, no. 5, pp. 953–959, Oct. 1999.
9) M. Reyes, P. Rodriguez, S. Vazquez, A. Luna, R. Teodorescu, and J. M. Carrasco, “Enhanced decoupled double synchronous reference frame current controller for unbalanced grid-voltage conditions,” IEEE Trans. Power Electron., vol. 27, no. 9, pp. 3934–3943, Sep. 2012.
10) A. Camacho, M. Castilla, J. Miret, A. Borrell, and L. de Vicuna, “Active and reactive power strategies with peak current limitation for distributed generation inverters during unbalanced grid faults,” IEEE Trans. Ind. Electron., vol. 62, no. 3, pp. 1515-1525, Mar. 2015.
11) A. Camacho, M. Castilla, J. Miret, J. Vasquez, and E. Alarcon-Gallo, “Flexible voltage support control for three phase distributed generation inverters under grid fault,” IEEE Trans. Ind. Electron., vol. 60, no. 4, pp. 1429–1441, 2013.
12) J. Miret, A. Camacho, M. Castilla, L. G. de Vicuna, and J. Matas, “Control scheme with voltage support capability for distributed generation inverters under voltage sags,” IEEE Trans. Power Electron., vol. 28, no. 11, pp. 5252–5263, Nov. 2013.

Author's Biography:

Thammathu Dhanasekhar Reddybabu, was born in Andhra Pradesh. He received the B.Tech degree in electrical and electronics engineering from JNTU Anantapur, in 2018, India. He is pursing M.Tech (Electrical Power Systems Student, Dept. Of Electrical And Electronics Engineering), Sri Venkateswara College Of Engineering And Technology (Autonomous), , Andhra Pradesh, And India)

Goduguchinta Venkat Pradeep was born in Andhra Pradesh, India. He received the B.Tech degree in Electrical and Electronics engineering from JNTU, Hyderabad in 2007. He received the M.Tech degree in High Voltage Engineering (HVE) from JNTU, Kakinada in 2010. Presently, he is working as an assistant professor with 10years of experience in Department of Electrical and Electronics Engineering at Sri Venkateswara college of Engineering &Technology(Autonomous), Chittoor, Andhra Pradesh, India.